Mon. Not. R. Astron. Soc. (2006) doi:10.1111/j.1365-2966.2006.10839.x

Lines in the cosmic microwave background spectrum from the epoch of cosmological hydrogen recombination

J. A. Rubiño-Martín,[1,2⋆] J. Chluba[2⋆] and R. A. Sunyaev[2,3]

[1]*Instituto de Astrofísica de Canarias, C/Vía Láctea s/n, E-38200 Tenerife, Spain*
[2]*Max-Planck Institut für Astrophysik, Karl-Schwarzschild-Str. 1, D-85740 Garching, Germany*
[3]*Space Research Institute (IKI), Russian Academy of Sciences, Moscow, Russia*

Accepted 2006 July 18. Received 2006 July 17; in original form 2006 April 28

ABSTRACT

We compute the spectral distortions of the cosmic microwave background (CMB) arising during the epoch of cosmological hydrogen recombination within the standard cosmological (concordance) model for frequencies in the range 1–3500 GHz. We follow the evolution of the populations of the hydrogen levels including states up to principle quantum number $n = 30$ in the redshift range $500 \leqslant z \leqslant 3500$. All angular momentum substates are treated individually, resulting in a total number of 465 hydrogen levels. The evolution of the matter temperature and the fraction of electrons coming from He II are also included. We present a detailed discussion of the distortions arising from the main dipolar transitions, for example Lyman and Balmer series, as well as the emission due to the two-photon decay of the hydrogen 2s level. Furthermore, we investigate the robusteness of the results against changes in the number of shells considered. The resulting spectral distortions have a characteristic oscillatory behaviour, which might allow experimentalists to separate them from other backgrounds. The relative distortion of the spectrum exceeds a value of 10^{-7} at wavelengths longer than 21 cm. Our results also show the importance of detailed follow-up of the angular momentum substates, and their effect on the amplitude of the lines. The effect on the residual electron fraction is only moderate, and mainly occurs at low redshifts. The CMB angular power spectrum is changed by less than 1 per cent. Finally, our computations show that if the primordial radiation field is described by a pure blackbody, then there is no significant emission from any hydrogen transition at redshifts greater than $z \sim 2000$. This is in contrast to some earlier works, where the existence of a 'pre-recombination' peak was claimed.

Key words: atomic processes – cosmic microwave background – cosmology: theory – early Universe.

1 INTRODUCTION

In the last twenty years, many experiments have been devoted to the study of the angular fluctuations of the cosmic microwave background (CMB) temperature and polarization. Nowadays, the results of the *WMAP* satellite (Spergel et al. 2003, 2006) in conjunction with other data sets (observations of Type Ia supernovae or galaxy surveys) give us the most precise determinations of the cosmological parameters describing our Universe, and constitute one of the most important confirmations of the hot Big Bang theory.

One of the predictions of this theory is the existence of small spectral distortions of the CMB blackbody spectrum arising as a consequence of the non-equilibrium conditions occurring during the epoch of the primordial hydrogen recombination at redshift $z \sim 1100$ (Zeldovich, Kurt & Syunyaev 1968; Peebles 1968).

These authors showed that, because in the Wien part of the CMB spectrum the brightness is extremely low, the strongest distortions are connected with the Lyα line (which today should be found at $\lambda \sim 170\,\mu$m), and with the 2s level two-photon decay emission (which should peak around $\lambda \sim 200\,\mu$m).

There should also be similar signatures arising from the recombination of helium (which occurs around $z \sim 6000$ for He III and $z \sim 2500$ for He II), but these appear at longer wavelengths than the hydrogen Lyα line (e.g. Dubrovich & Stolyarov 1997; Wong, Seager & Scott 2006) and they lie one order of magnitude below the hydrogen spectrum, just due to the lower abundance of helium.

Dubrovich (1975) proposed to look for the spectral distortions due to transitions between higher levels of the hydrogen atom (Balmer and higher series), and after this, many papers were devoted to the problem of the formation of the hydrogen recombination

⋆E-mail: jose.alberto.rubino@iac.es (JAR-M); jchluba@mpa-garching.mpg.de (JC)

lines in the early Universe (Liubarskii & Sunyaev 1983; Rybicki & dell'Antonio 1993; Dubrovich & Stolyarov 1995, 1997; Boschan & Biltzinger 1998; Burgin 2003; Dubrovich & Shakhvorostova 2004; Kholupenko, Ivanchik & Varshalovich 2005; Wong et al. 2006). Although there were contradictory results in the amplitudes and shapes of the features, these computations showed that the amplitude of the spectral distortions arising from transitions of the higher series is very small, with typical values around $\sim 10^{-6}$–10^{-8}. The important point for us is that these distortions should have survived until today and might become observable in the near future.

The measurements from the Far-InfraRed Absolute Spectrophotometer (FIRAS, e.g. Fixsen et al. 1996; Fixsen & Mather 2002) on board the *COBE* satellite indicate that the CMB frequency spectrum is described by a $T_0 = 2.725 \pm 0.001$ K blackbody spectrum with high precision. The limits on the Bose–Einstein and Compton distortions are $|\mu| < 9 \times 10^{-5}$ (95 per cent CL) and $|y| < 15 \times 10^{-6}$ (95 per cent CL), respectively. Moreover, Fixsen & Mather (2002) pointed out that recent technological progress permits one to improve the limits by nearly two orders of magnitude. Therefore, we are approaching the sensitivities required for detecting global features in the spectrum, so detecting individual ones could be possible in the next future. Therefore, precise computations of the shapes, positions and amplitudes of these lines are needed. We also mention that there have been attempts to measure the CMB spectrum at centimetre wavelengths using the *ARCADE* experiment (Fixsen et al. 2004; Kogut et al. 2004).

In most of the existing calculations simplifying assumptions have been used in order to make the problem computationally tractable. For the study of the Lyα line and the 2s two-photon decay emission, the effective three-level atom is usually adopted (e.g. Peebles 1968; Zeldovich et al. 1968; Boschan & Biltzinger 1998; Wong et al. 2006). For transitions in the Balmer and higher series, two assumptions are usually adopted (e.g. Burgin 2003; Dubrovich & Shakhvorostova 2004; Kholupenko et al. 2005). First, a quasi-static evolution of the populations for all levels above $n = 2$ is assumed, which reduces the problem of solving a system of stiff-coupled ordinary differential equations to an algebraic system. And secondly, given that one of the main difficulties is treating *all* the energetically degenerate angular momentum sublevels within each shell, only the total population of a given shell is computed and statistical equilibrium (SE) among the sublevels is assumed. To date, the only attempt to avoid these two assumptions was made by Rybicki & dell'Antonio (1993), who considered the case of 10 shells. However, their results were not conclusive and were affected by numerical uncertainties. In particular until now the question whether the assumption of SE is justified has not been addressed satisfactorily.

It is important to mention that all the codes which compute the power spectrum of the angular fluctuations of the CMB make use of the recombination history as obtained with the RECFAST code (Seager, Sasselov & Scott 1999). These calculations are based on a 300-level hydrogen atom in which SE among the l sublevels was assumed (Seager, Sasselov & Scott 2000). Therefore, it would also be important to understand the validity of this approximation and its effects on the recombination history.

In our paper, we have obtained the spectral distortions from *all lines* of hydrogen including 30 shells, following the evolution of all angular momentum substates separately. Since we are until now not including collisions, from an estimate following Pengelly & Seaton (1964) this seems a natural choice in order to keep the calculations simple. Our Universe has extremely high entropy, that is, photons outnumber the baryons by a factor of $\sim 1.6 \times 10^9$. This is why collisions in general are *not* important. However, those collisions connecting different, energetically degenerate angular momentum substates within a given shell should play a role for sufficiently high shells, but the results presented here should remain unaffected. A detailed discussion of this subject will be done in a subsequent paper (Chluba, Rubiño-Martin & Sunyaev 2006).

Our computations have permitted us to show for the first time that the deviations in the populations of the angular momentum substates within a given shell from SE are important when studying the spectral distortions to the cosmological blackbody, and that the impact on the residual ionization fraction of the hydrogen atoms after recombination is of the order of a few per cent. However, this change is sufficiently important to produce modifications of the order of a few per cent on the predicted angular power spectrum, so this effect should be taken into account for future experiments like *Planck*.

The main results of this paper are summarized in Figs 1 and 2. The hydrogen lines from the epoch of cosmological recombination appear as broad ($\Delta\nu/\nu \approx 0.30$–$0.40$) features, having high contrast for the Lyman, Balmer, Paschen, Brackett and Pfund series. Altogether they produce a spectral distortion with a characteristic oscillatory behaviour, which cannot be mimicked by any other foreground, and thus might be used in order to devise a method for their detection. Although most of the current observational efforts are dedicated to the study of the (temperature and polarization) angular fluctuations, it is clear that measuring these spectral features would constitute a unique way to test our understanding of the recombination process. For example, it will provide a *direct* determination of the redshift of recombination, and independent determinations of cosmological parameters such as the baryon density. One should mention that the broadening due to the scattering off free electrons in the epoch of recombination is at most of the order of a few per cent (e.g. Dubrovich & Stolyarov 1997), implying that the features we are discussing in this paper are not going to be wiped out.

Cosmological recombination cannot produce many more than one photon per transition in the hydrogen atom per one act of recombination. This fact, together with the high entropy of the Universe, are the reasons why only in two extreme cases might the spectral distortions connected with the cosmological hydrogen recombination become observable in the future: (i) the Wien part of the CMB spectrum (Lyα, 2s two-photon decay emission and the Balmer lines) and (ii) the Rayleigh–Jeans part.

Concerning the first case, the cosmic infrared background (CIB) appears six orders of magnitude above the signals we are discussing, so the detection in the Wien part of the spectrum will be challenging. On the other hand, at very low frequencies the foregrounds like the 21-cm line, synchrotron emission of relativistic electrons of radio and ordinary galaxies become important and make observations more complicated. From this point of view the spectral band $\nu \gtrsim 1.4$ GHz is more interesting, because the 21-cm emission will not contaminate in this frequency range, and the relative amplitude of the distortions in this band becomes larger (of the order of $\sim 10^{-7}$).

This paper is organized as follows. In Section 2 we briefly review the assumptions of the computations of this paper, as well as the basic equations. Section 3 presents the results for the complete spectrum

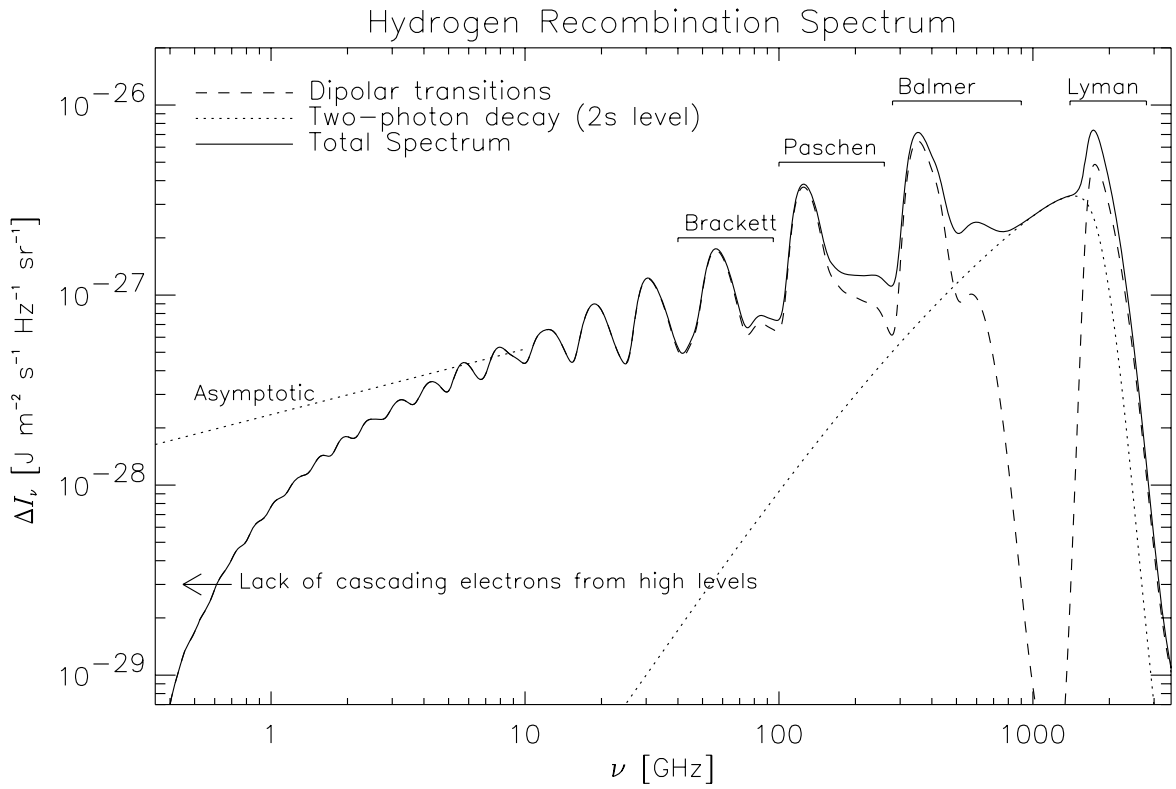

Figure 1. Full hydrogen recombination spectrum for $n_{\rm max} = 30$. The populations of all the angular momentum substates were taken into account. We indicated the contributions corresponding to the Lyman, Balmer, Paschen and Brackett series. The straight line shows one possible asymptotic behaviour at low frequencies when including higher hydrogen shells (see text for details).

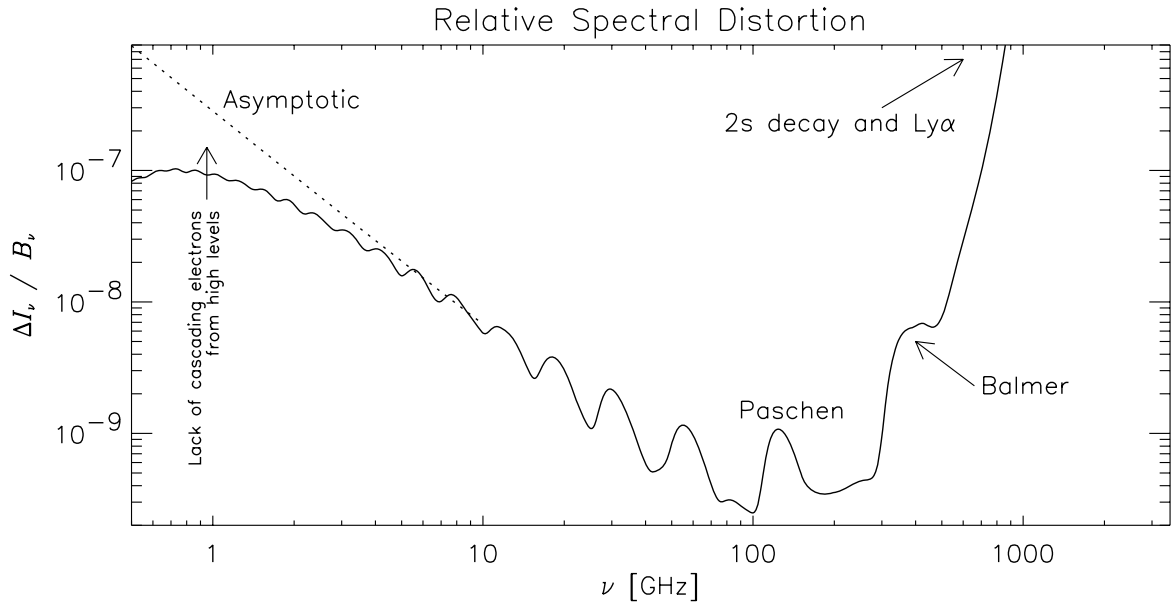

Figure 2. Relative spectral distortion of the CMB spectrum for the hydrogen recombination spectrum as computed in this paper. We use the same frequency range as in Fig. 1. Note that the Lyα and two-photon decay features produce very strong relative distortions which exceed unity, so they are not presented here for clarity.

and for individual lines. In that section we discuss the robustness of the results when changing the total number of shells, as well as the non-equilibrium effects arising from the angular momentum states. Sections 4 and 5 present the discussion and the conclusions, respectively.

2 BASIC EQUATIONS

In order to calculate the time-evolution of the populations of the multilevel hydrogen atom, we adopt the procedure described in Seager et al. (2000). Here, we would like to emphasize

the most important assumptions that this approach implies as follows.

(i) The observed deviations of the CMB spectrum from a blackbody are smaller than $\Delta I/I_0 \lesssim 10^{-4}$ (Mather et al. 1994; Fixsen et al. 1996). Therefore, the radiation field is assumed to be described by a perfect blackbody with temperature $T_0 = 2.725\,\mathrm{K}$.

(ii) The quasi-static solution for the spectral line profiles is valid (Rybicki & dell'Antonio 1994).

(iii) The Sobolev escape probability method (Sobolev 1946) is adopted to deal with the evolution of all lines [see Dubrovich & Grachev (2004) for a derivation of this method in a cosmological context]. In practice, this will only affect those transitions which are directly connecting with the ground state, while for the rest the optical depths τ_ν are so small that the escape probability is very close to unity. Therefore, it is possible to work in the optically thin limit taking into account only terms proportional to τ_ν for the corresponding transition (Rubiño-Martín, Hernández-Monteagudo & Sunyaev 2005).

In our computation, the major differences with respect to the Seager et al. (2000) procedure are the following.

(i) We split the hydrogen levels up according to their *principal* and *angular momentum* quantum numbers (n, l) and include *all* sublevels. To illustrate the dependence of the recombination spectrum on the treatment of the angular momentum substates, we also consider some cases, in which we follow the populations of *all* sublevels with $n \leqslant n_{\rm sp}$, while for levels with $n_{\rm sp} < n \leqslant n_{\rm max}$ we average over the angular momentum states [i.e. we assume that the sublevels are populated according to their statistical weights, so that $N_{nl} = (2l + 1)\,N_{ns}$ is fulfilled]. This implies that for given $n_{\rm sp}$ and $n_{\rm max}$ we follow the populations of $N = n_{\rm sp}\,[n_{\rm sp}+1]/2 + n_{\rm max} - n_{\rm sp}$ separate hydrogen states.

(ii) We neglect collisional rates, as they have been found to be of minor importance (Seager et al. 2000).

(iii) We only follow the He II ionization fraction without any detailed follow-up of separate levels.

(iv) Instead of directly tracking the physical population N_i of a level i we define the variables $X_i = N_i/N_{\rm H}$, where $N_{\rm H}(z)$ is the total number density of hydrogen nuclei in the universe. In this way one can absorb the expansion term.

A very similar treatment has been used in Rubiño-Martín et al. (2005) to calculate the imprints of the cosmological hydrogen recombination lines on the CMB angular power spectrum including all sublevels up to $n_{\rm max} = 10$. Here, we developed two independent codes using different routines of the NAG Library to solve the system of stiff ordinary differential equations. The results of both codes were absolutely consistent and robust.

In addition, we explored three different numerical methods to compute the photoionization and photorecombination rates: the approximations (valid for small values of the energy of the ejected electron) given by Burgess (1958); the polynomial expressions given by Karzas & Latter (1961) and Boardman (1964); and the numerical subroutines provided by Storey & Hummer (1991). The second and third approaches were found to give identical results for all levels up to $n_{\rm max} = 30$. Even though the approximations adopted by Burgess (1958) are not valid for high values of n and frequencies far away from the photoionization threshold of each transition, we found that for the calculations of this paper ($n_{\rm max} \leqslant 30$), they yield similar results (within a few per cent accuracy) with respect to those obtained in the other two cases. It also turned out that the inclusion of induced photorecombination is important for the brightness of those transitions with $\Delta n = 1$ at high levels ($n \gg 1$). Finally, we mention that we have also explored simple formulae for the computation of the photoionization/photorecombination cross-sections, as those obtained using the Kramers approximation, in which the Gaunt factors are neglected. We found that this kind of approximation is *not* reproducing properly the trends within a given shell, overestimating the rates which are connecting those sublevels with very high l-values to the continuum.

For all the computations presented in this work, the following values of the cosmological parameters were adopted (Bennett et al. 2003): $\Omega_{\rm b} = 0.0444, \Omega_{\rm tot} = 1, \Omega_{\rm m} = 0.2678, \Omega_\Lambda = 0.7322, Y_{\rm p} = 0.24$ and $h = 0.71$.

2.1 Hydrogen spectral distortions due to radiative dipole transitions

In order to calculate the spectral distortions arising from the hydrogen dipole transitions we use a δ-function approximation for the line-profile, that is, we neglect any lifetime effects (Lorentz profile) or thermal broadening (Voigt profile). A straightforward derivation yields the spectral distortion, $\Delta I_{ij}(\nu)$, arising form the transition of the upper level i to the lower level j (e.g. also see Wong et al. 2006):

$$\Delta I_{ij}(\nu) = \frac{ch}{4\pi}\frac{\Delta R_{ij}(z_{\rm em})}{H(z_{\rm em})[1+z_{\rm em}]^3}, \tag{1}$$

where $z_{\rm em}$ is the redshift of emission, which relates the observing frequency ν to the transition frequency ν_{ij} by $\nu = \nu_{ij}/[1+z_{\rm em}]$. Furthermore H denotes the Hubble factor and the effective radiative rate for the considered transition is given by

$$\Delta R_{ij} = p_{ij}\,\frac{A_{ij}\,N_i\,\mathrm{e}^{h\nu_{ij}/kT_\gamma}}{\mathrm{e}^{h\nu_{ij}/kT_\gamma}-1}\left[1-\frac{g_i}{g_j}\,\frac{N_j}{N_i}\,\mathrm{e}^{-h\nu_{ij}/kT_\gamma}\right], \tag{2}$$

where p_{ij} is the Sobolev-escape probability as defined in Seager et al. (2000), A_{ij} is the Einstein-A-coefficient of the transition, N_i and g_i are the population and statistical weight of the upper and N_j and g_j of the lower hydrogen level, respectively. Furthermore, we have assumed that the ambient photon field is given by a blackbody spectrum with temperature $T_\gamma = T_0[1+z]$, where $T_0 = 2.725$ K is the present CMB temperature (Fixsen & Mather 2002), and we have made use of the Einstein relations.

2.2 Hydrogen 2s–1s spectral distortion

The spectral distortion arising due to the two-photon decay of the hydrogen 2s level can be obtained by the integral (e.g. see Zeldovich et al. 1968; Wong et al. 2006):

$$\Delta I_{\rm 2s1s}(\nu) = \frac{ch\nu}{4\pi}\int_0^\infty \frac{\Delta R_{\rm 2s1s}(z)\,\phi(\nu[1+z]/\nu_\alpha)}{H(z)[1+z]^3}\,\mathrm{d}z. \tag{3}$$

Here $\Delta R_{\rm 2s1s} = A_{\rm 2s1s}\,[N_{\rm 2s} - N_{\rm 1s}\mathrm{e}^{-h\nu_\alpha/kT_\gamma}]$, where the total two-photon decay rate for the hydrogen 2s level is given by $A_{\rm 2s1s} = 8.22458\,\mathrm{s}^{-1}$ and $\nu_\alpha \approx 2.46\times10^{15}$ Hz is the Lyα photon frequency.

A definition of the profile function $\phi(y)$ can be found in Spitzer & Greenstein (1951) but a sufficient approximation was obtained by Nussbaumer & Schmutz (1984) as

$$\phi(y) = \frac{C}{\nu_\alpha}\left[w(1-4^\gamma\,w^\gamma) + \alpha\,w^{\beta+\gamma}\,4^\gamma\right], \tag{4}$$

Table 1. Positions and amplitudes of the main features shown in Fig. 1. We show the central frequency (ν_0) and wavelength (λ_0) as observed today, the relative width at half maximum ($\Delta\nu/\nu$) and the peak intensity for the features corresponding to the first five series of hydrogen. For comparison, the last five columns show the central redshift of formation, the central frequency, the relative width, the peak and relative amplitude of the corresponding α-transition (i.e. $\Delta n = 1$) when considered separately.

Series	n	ν_0 (GHz)	λ_0 (μm)	$\Delta\nu/\nu$	ΔI_ν(peak) (J m^{-2} s^{-1} Hz^{-1} sr^{-1})	z_α	ν_α (GHz)	$(\Delta\nu/\nu)_\alpha$	ΔI_α (J m^{-2} s^{-1} Hz^{-1} sr^{-1})	$\Delta I_\alpha/\Delta I_\nu$ (per cent)
Lyman	1	1732	173	0.28	7.4×10^{-27}	1407	1752	0.23	4.8×10^{-27}	65
Balmer	2	353	849	0.37	7.2×10^{-27}	1274	358	0.26	6.5×10^{-27}	93
Paschen	3	125	2398	0.31	3.8×10^{-27}	1259	127	0.26	3.3×10^{-27}	87
Brackett	4	56	5353	0.36	1.8×10^{-27}	1304	57	0.27	1.2×10^{-27}	67
Pfund	5	30	9993	0.39	1.2×10^{-27}	1312	31	0.27	7.3×10^{-28}	61

where $w = y[1 - y], C = 24.5561, \alpha = 0.88, \beta = 1.53$ and $\gamma = 0.8$. Here, it is important to note that $\phi(y)$ is normalized to $\int_0^{\nu_\alpha} \phi(\nu/\nu_\alpha)\,\mathrm{d}\nu = 2$ in order to account for the fact that *two* photons are emitted per decay of *one* hydrogen 2s level (see also Boschan & Biltzinger 1998).

3 RESULTS

3.1 The full recombination spectrum

In Figs 1 and 2, we present the full hydrogen recombination spectrum for $n_{\rm max} = 30$. The population dependence on l was taken into account for all shells ($n_{\rm sp} = 30$). In this calculation, the evolution of 465 separate hydrogen states in the redshift range of $500 \leqslant z \leqslant 3500$ was included.

At high frequencies, one can clearly see the features corresponding to the Lyman, Balmer, Paschen and Brackett series. We will discuss some of these lines in more detail below. At lower frequencies, the lines start to overlap strongly and eventually merge to a continuum at very low ν. The figure also shows one *possible* asymptotic behaviour at low frequencies. This is meant to illustrate the fact that, when including a larger number of shells, the additional cascading electrons will enhance the emission at low frequencies. Here, we decided to plot this asymptotic limit using the slope of Kholupenko et al. (2005). These authors were the first to obtain the spectral distortions for a very high number of levels ($n_{\rm max} = 160$), although under the assumption of quasi-static evolution and without taking into account the populations of the angular momentum substates separately. Their average slope in the 1–10 GHz range is approximately +0.35, while in our case, the average slope in the frequency range 2–10 GHz has a value of approximately +0.8. A detailed discussion of this asymptotic region requires the inclusion of several physical effects which have not been treated in this paper. For example, it is clear that even at lower frequencies free–free absorption will start to erase any emission from the very high hydrogen levels, and in addition collisions should become important. Therefore, the study of the low-frequency asymptotic region will be left for a subsequent paper. However, we expect that the value of the slope obtained from the paper of Kholupenko et al. (2005) provides a lower limit.

Table 1 summarizes some parameters (peak amplitude, central frequency and relative width) of the first five features in the complete (including the 2s decay line) spectrum presented in Fig. 1. It is interesting to compare these values with those for the corresponding α-transition ($\Delta n = 1$). Clearly, the main contribution to the features comes from this line, although the emission due to the 2s decay is significant in the range of the Lyman series. Furthermore, the width of the features is slightly increased with respect to the α-line due to the addition of higher transitions ($\Delta n > 1$), and in the case of the Lyman and Balmer features, because of the 2s-decay emission.

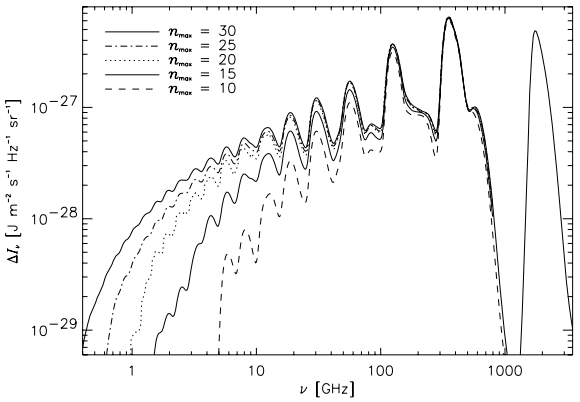

Figure 3. Hydrogen recombination spectrum for different values of $n_{\rm max}$. The contribution from the 2s two-photon decay was not shown on this plot. We show the cases of $n_{\rm max} = 10, 15, 20, 25$ and 30, always with $n_{\rm sp} = n_{\rm max}$.

3.1.1 *Dependence on the number of shells*

At frequencies $\nu \lesssim 2$ GHz, the slope of the computed spectrum changes significantly. This is due to the lack of diffusion of electrons from levels above $n_{\rm max}$ and transitions from those levels with $\Delta n > 1$, which have not been accounted for here. In order to estimate this effect we have performed additional calculations with $n_{\rm max} = 10, 15, 20$ and 25, all for $n_{\rm sp} = n_{\rm max}$. A compilation of the results is shown in Fig. 3. One can see that the lines of the Lyman, Balmer, Paschen and Brackett series basically do not change when increasing the number of shells beyond $n_{\rm max} \sim 20$. On the other hand, the low-frequency part ($\nu \lesssim 10$ GHz) is still varying rather significantly. Our calculations suggest that for $n_{\rm max} = 30$ at the level of a few per cent the spectrum is converged for $\nu \gtrsim 20$ GHz even when adding more shells. Pushing $n_{\rm max}$ to larger values should lead to an increase of the distortions at low frequencies and eventually should partially fill the gap with respect to the asymptotic behaviour indicated in Fig. 1.

3.1.2 *Non-equilibrium effects of the angular momentum states*

Most of the computations of the hydrogen recombination spectrum published to date were either based on the effective three-level atom (e.g. Boschan & Biltzinger 1998; Wong et al. 2006), or used averaging over angular momentum sublevels (e.g. Dubrovich & Grachev 2004; Kholupenko et al. 2005). Here, we will discuss the influence of the latter simplification on the solution obtained for the recombination spectrum.

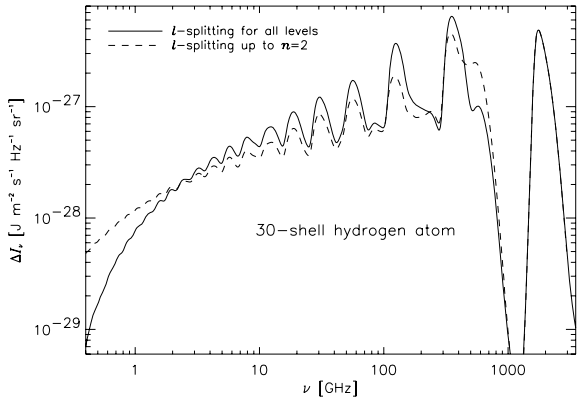

Figure 4. Non-equilibrium effects of the angular momentum states on the hydrogen recombination spectrum. We consider the case $n_{\rm max} = 30$ for two different values of $n_{\rm sp}$ as indicated in the legend. The contribution from the 2s two-photon decay was omitted here.

Fig. 4 compares our result for $n_{\rm sp} = 30$ with the case of $n_{\rm sp} = 2$ (which represents the standard computation without detailed follow-up of the l-substates except for the 2s and 2p levels).

The 'non-splitting' solution has a higher intensity at frequencies smaller than $\nu \sim 2$ GHz and also a smaller slope in this region. This shows that, for a hydrogen atom with given $n_{\rm max}$, the $n_{\rm sp} = 2$ solution is effectively having a larger number of transitions in the upper shells (i.e. higher diffusion), resulting in an excess of emission. We will come back to this point below. In addition, there are also effects on the high-frequency part of the spectrum. For $n_{\rm sp} = 2$, the peak intensities of the main transitions ($\Delta n = 1$) are underestimated while the ratios of the main to the secondary transitions ($\Delta n > 1$) are decreased. In other words, the incomplete treatment of the high levels also affects the diffusion to lower levels, and hence the line intensities are affected as well.

For example, the Balmer lines of the spectrum are strongly affected. The ratio of the two peaks appearing at ∼350 and ∼550 GHz (which correspond to Hα and a superposition of lines higher than Hγ, respectively; see the section on Balmer lines) decreases from roughly 6 to about 2, and the height of the smaller peak is more than two times bigger than that in the full calculation.

We note that a comparison of our results for $n_{\rm sp} = 2$ with those obtained by Kholupenko et al. (2005) shows a very good correspondence. When doing the computations using their cosmological parameters, we find good agreement also in the amplitudes, showing that our two implementations can produce similar results. Given that these authors produced their spectrum assuming a quasi-static evolution for all shells above $n = 2$, our results further support the idea that their approach is appropriate (see also the comments in Dubrovich & Shakhvorostova 2004). However, including the evolution of the populations of all l-substates in this approach seems more difficult to solve, because the deviations from SE within a shell are very small, and the corresponding columns in the matrix of the level populations will be degenerated. To test this point, we have also implemented the quasi-static approach for shells $n > 2$, while solving the evolution (differential equations) for $n \leqslant 2$ and the electron fraction. For our implementation of the problem, we found that, when considering all the angular momentum substates separately, with standard methods solving the complete set of ordinary differential equations seems more efficient (in terms of computational time) than solving the corresponding algebraic system.

Finally, we have also performed several computations considering values of $n_{\rm sp}$ in the range between 2 and $n_{\rm max}$, mainly with the aim of understanding whether the full computations could be simplified. In these cases, we found that the spectrum obtained is closer to the full solution ($n_{\rm sp} = n_{\rm max}$) in the high-frequency part. However, there always appears an abrupt change of slope in the spectrum precisely at the frequency corresponding to the main transition of the $n_{\rm sp}$ series. Below this frequency, the average slope of the spectrum is flatter than that in the full solution.

Obviously, all the effects discussed in Fig. 4 appear because the inclusion of l-substates modifies the populations of the levels. In order to understand these modifications, and how the differences in the populations of the levels are connected with changes in the spectral distortions, we will now discuss these effects in detail.

Effects within a given shell. We first discuss the situation for a given shell (i.e. we fix n), where we compare the populations of the different sublevels with the corresponding expected value in the case of SE within the shell, that is, when $N_{nl}^{\rm SE} = [(2l+1)/n^2]\, N_{\rm tot}$, where $N_{\rm tot}$ is the (actual) total population of the shell.

In Fig. 5, we present the ratios $N_{nl}/N_{nl}^{\rm SE}$ of the true population N_{nl} of the level for the full computation with $n_{\rm max} = 30$, to the expected SE population. We show six different cases, corresponding to values of the principal quantum number $n = 3, 5, 10, 15, 20$ and 25. For each one of these cases, we present the ratios at three different redshifts ($z = 1200$, 1300 and 1400) which correspond to the region where the lines are forming. At higher redshifts, the deviations from SE show a similar trend, but they are much smaller in amplitude and tend to disappear. This behaviour is expected since one is then approaching the epoch of full thermodynamic equilibrium (Zeldovich et al. 1968). In our calculations, the non-equilibrium effects are compatible with zero within the numerical precision of the two codes at $z \gtrsim 2000$.

The general trend for all shells above $n = 5$ can be summarized as follows: within a given shell the sublevels with $l \lesssim 5$–6 are underpopulated as compared to $N_{nl}^{\rm SE}$, with the difference being the strongest for the d level ($l = 2$) and smallest for the level $l \sim 5$–6. This shows that in the calculations with full follow-up these angular momentum states depopulate faster. For $l > 6$, the population of the substates is larger than that in the SE situations. This implies that these angular momentum states depopulate slower, which is likely due to blocking of the transition to lower levels ($\Delta l = \pm 1$ restriction). On the other hand, for those shells $n \leqslant 5$, the p and d levels are also underpopulated, but now the strongest deviation appears for p level ($l = 1$). When comparing our results for $n_{\rm max} = 30$ with the case of $n_{\rm max} = 25$ and 20, we can conclude that the results in Fig. 5 for $n \leqslant 10$ have already converged, but higher shells could increase their deviations from SE, especially at high l-states.

Although the explanation of these non-equilibrium effects requires one to study the net rates for all transitions connecting to that particular level, we can understand some of the general trends with the following arguments. It is clear that assuming SE is equivalent to 'instantaneous' redistribution within a given shell, that is, if an electron is captured by a given l-state, this will immediately increase the population of *all* the other l-states. One would expect that instantaneous redistribution will operate when collisions $(n, l) \rightarrow (n, l')$ are effective. This should eventually happen in sufficiently high shells (see Section 4). On the other hand, when instantaneous redistribution is not working, then the depopulation of each level will depend on the exact route the electron can take to reach the ground state.

As the Universe expands, the blackbody radiation field is redshifting to lower energies, and thus the number density of high-energy photons decreases with time. When the radiation field does not con-

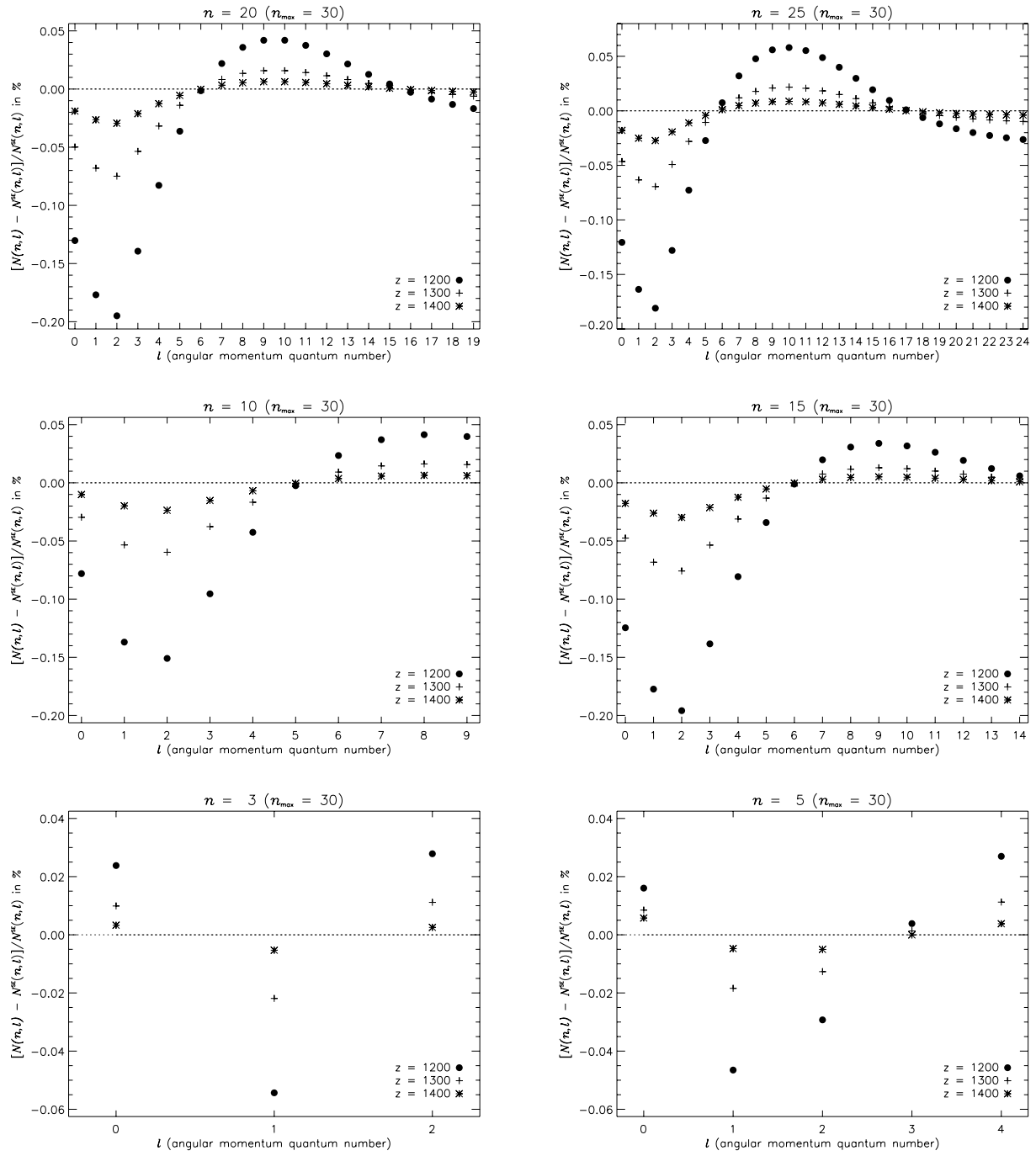

Figure 5. Non-equilibrium effects on the populations of the angular momentum substates for a given n. The results were obtained for $n_{\max} = 30$ following the populations of all the angular momentum substates. We present the ratio $N_{nl}/N_{nl}^{\rm SE}$, where the SE population is computed from the actual total population of the shell by $N_{nl}^{\rm SE} = [(2l+1)/n^2]\,N_{\rm tot}$. Six cases are shown, corresponding to values of the principal quantum number n= 3, 5, 10, 15, 20 and 25.

tain enough photons to maintain equilibrium in a given shell n (i.e. when the number of photons with energy above the photoionization potential of the shell χ_n falls below 1 per atom), then the photoionization rates become smaller than the photorecombination rates and the electrons cannot escape to the continuum. Note that this is first happening for lower shells with the largest photoionization potential.

In the above situation, the electrons try to cascade down to lower levels. Our computation only includes radiative rates, so electrons in a given shell can only diffuse down through transitions with $\Delta l = 1$. In general, it seems that the fastest transitions are found to be those which can directly connect with the 2s and 2p levels, so it is reasonable to expect that all sublevels with $l \leqslant 2$ will be able to depopulate faster in the complete ($n_{\rm sp} = n_{\max}$) computation, and their SE populations will seem larger. On the other hand, due to the bottleneck, which is produced in the lower states during cosmological recombination, states with high values of l depopulate slower

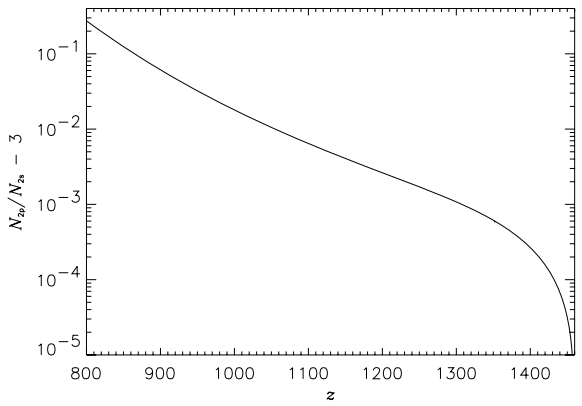

Figure 6. Non-equilibrium effects in the populations of the 2s and 2p levels. We present the ratio of the 2s and 2p populations referred to the equilibrium ratio (i.e. the statistical weights), as a function of redshift. Although the deviations are very small, they indicate that there is a deficit of electrons in the 2s state as compared to the 2p state as a consequence of the recombination dynamics.

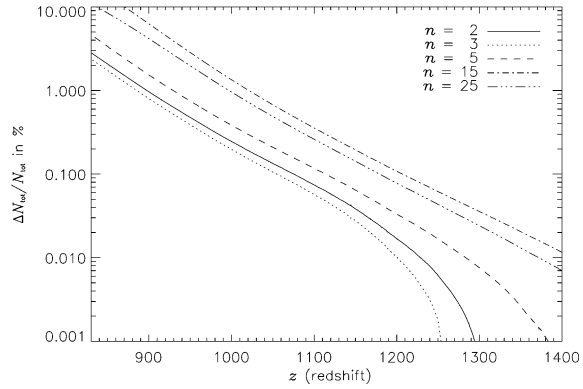

Figure 7. Non-equilibrium effects in the populations of the levels for different values of n. We present the relative change in the total population of the levels $[N_{\rm tot}(n) = \sum_l N_{nl}]$ due to the detailed follow-up of the angular momentum substates, for a hydrogen atom with $n_{\rm max} = 30$. Note that the fractional change, defined as $[N_{\rm tot}^{(n_{\rm sp}=n_{\rm max})} - N_{\rm tot}^{(n_{\rm sp}=2)}]/N_{\rm tot}^{(n_{\rm sp}=2)}$, is always positive, so that the total population of a given shell in the calculations for $n_{\rm sp} = n_{\rm max}$ is always larger than for $n_{\rm sp} = 2$.

in the full computation, since electrons have to cascade down via many intermediate shells.

Finally, we also present in Fig. 6 the ratio of the populations of the levels 2s and 2p as a function of redshift. This figure quantifies the fact that at high redshifts, both the 2s and 2p populations are in SE, so their population ratio equals the ratio of the statistical weights. However, as the recombination proceeds, deviations from the equilibrium appear, in the sense that there is an overpopulation of the 2p level with respect to the 2s level because the main channel of recombination at low redshifts ($z \lesssim 1400$) is the 2s two-photon decay. We will return to this point in Sections 3.2 and 3.3.

Effects on the total population of different shells. The effects connected with the departure from SE within a given shell are not only visible for different substates, but also produce a net effect on the overall population of the level. We illustrate this point in Fig. 7, where we present the relative change of the overall population of a given shell for $n_{\rm max} = n_{\rm sp}$, with respect to the standard ($n_{\rm sp} = 2$) computation.

For a given shell n, the total population (sum over all l-states) in the computations with $n_{\rm sp} = n_{\rm max}$ is always larger than for $n_{\rm sp} = 2$. This shows that in general the overall depopulation of a given shell is slower for full follow-up. Moreover, for $n > 3$ the relative difference becomes larger when increasing the value of n (for $n = 3$, the net effect is slightly smaller than that for level $n = 2$). For high values of n (close to $n_{\rm max}$), this relative change seems to decrease again as a consequence of the lack of diffusion from higher shells.

At low redshifts $z \lesssim 900$, the relative difference becomes larger than 1 per cent for all the levels. On the other hand, in the redshift range where the spectral distortions are produced (e.g. for the main transitions, the redshift of formation is $z \sim 1300$ for high n, and $z \sim$1400 for $n = 2$), the fractional change is extremely small. This shows that the total population of the shell during the epoch of recombination does not depend significantly on the treatment of the angular momentum substates, although these small deviations are sufficient to produce the effects shown in Fig. 4.

Effects on the transitions between different shells. In this paragraph, we wish to understand the effects on the transition rates between different shells. Although the detailed analysis again would require one to show the differences in the net rate for each transition, we will show that using the results and arguments of the last two paragraphs we can understand the general trend and sign of the correction to the resulting spectral distortion as shown in Fig. 4.

When including l-substates, the populations of all levels will be given by $N_i \equiv N_i^{\rm ns} + \Delta N_i$, where we introduced $N_i^{\rm ns}$ referring to the populations in the case of 'non-splitting' in angular momentum above $n = 2$, that is, $n_{\rm sp} = 2$. Given that the optical depth for all transitions to levels above the ground state is very small (Rubiño-Martín et al. 2005), the escape probabilities p_{ij} are very close to unity and therefore will practically not change when following the populations of the l-substates. Thus, the net rate can be written as $\Delta R_{ij} = \Delta R_{ij}^{\rm ns}\,[1 + \Delta]$, where $\Delta R_{ij}^{\rm ns}$ is the rate as obtained in the calculation for $n_{\rm sp} = 2$. The function Δ is defined by

$$\Delta R_{ij}^{\rm ns} \times \Delta = \frac{\Delta N_j}{N_j^{\rm ns}} \left[\frac{(\Delta N_i/N_i^{\rm ns})}{(\Delta N_j/N_j^{\rm ns})} - \frac{g_i}{g_j}\,\frac{N_j^{\rm ns}}{N_i^{\rm ns}}\,{\rm e}^{-h\nu_{ij}/kT_\gamma} \right]. \qquad (5)$$

For simplicity, let us now only consider the α-transitions. These give the main contribution to the CMB spectral distortion and always lead to *positive* features (see Fig. 4), implying that

$$\Delta R_{ij}^{\rm ns} \propto \left[1 - \frac{g_i}{g_j}\,\frac{N_j^{\rm ns}}{N_i^{\rm ns}}\,{\rm e}^{-h\nu_{ij}/kT_\gamma} \right] > 0. \qquad (6)$$

Therefore, the sign of Δ will be defined by the right-hand side of equation (5).

Now, comparing equation (5) with (6) one can conclude that for $(\Delta N_i/N_i^{\rm ns})/(\Delta N_j/N_j^{\rm ns}) > 1$ the term within the brackets is positive, and could become negative if this ratio is smaller than 1. In addition, one has to check the sign of the factor $\Delta N_j/N_j^{\rm ns}$ to obtain the overall sign of Δ.

A detailed analysis would require one to study the sign and amplitude of these corrections for every one of the different channels contributing to a given transition. These numbers can in principle be derived by combining the information of Figs 5 and 7. However, it is clear that a better approach would be to directly study the net rates for every transition of interest. We will do that in the following subsections for some examples, although here we want to illustrate that one can understand the overall sign of the correction to the spectral distortions with this argument.

If we apply equation (5) to the *total* populations of the two levels that we are connecting (this means that we neglect the deviations from SE within the shell as have been discussed above), then we

can use Fig. 7 to understand the net sign of the correction. All the fractional changes in Fig. 7 are positive, so we only need to consider the ratio between the levels involved in the transition. On one hand, for $2 < n \lesssim 20$ the relative population is growing with n, so equation (5) shows that the correction term to the net rate should be positive, and thus the spectral distortion in the full computation lies above the result for non-splitting. However, for high n-values (close to $n_{\rm max}$), Fig. 7 shows that $(\Delta N_i/N_i^{\rm ns})/(\Delta N_j/N_j^{\rm ns})$ can be expected to be less than unity for $n \gtrsim 20$, implying that the term in equation (5) inside the brackets can eventually become negative, and thus the spectral distortion in the full computation will lie below the non-splitting solution at low frequencies.

We note that the above argument is only used here to show the qualitative behaviour of the correction when taking into account angular momentum substates. In our real computations, we considered all possible radiative channels (and hence all possible sublevels), which contribute to a given transition, so a detailed analysis based on the net rates ΔR_{ij} for all channels would in principle be possible.

3.2 The Lyα line

As found by other authors, the Lyα line leads to the strongest distortion of the CMB spectrum and appears in the Wien tail of the blackbody spectrum. In our computations, it peaks at wavelength around 170 μm (see Fig. 8 and Table 1) and is very similar in shape and amplitude to the results obtained by Wong et al. (2006). However, as discussed below, we do not find any pre-recombination peak.

In Fig. 9, we present several transitions with $\Delta n = 1$ in redshift space. The figure shows that the bulk of the Lyα emission originates around $z \approx 1400$, as obtained by other authors (e.g. Liubarskii & Sunyaev 1983). Increasing n one can see that the corresponding transition, due to the decrease in the transition energy, stays longer in equilibrium with the photon field. However, when the transition frequency close to the decoupling redshift (i.e. the redshift at which the corresponding line starts appearing) drops below the maximum of the CMB spectrum {here in terms of photon number, $N_\nu \propto \nu^2/[\exp(h\nu/kT_\gamma) - 1]$}, that is, $\nu_{\rm max} \sim 90.3 \times (1+z)$ GHz, then increasing n further will shift the redshift of formation for the corresponding line back to larger z (see Fig. 9 transition $10 \rightarrow 9$). For a more quantitative estimate, one also has to include the dependence of A_{ij} on n and eventually will end up looking at the net transition rates in more detail.

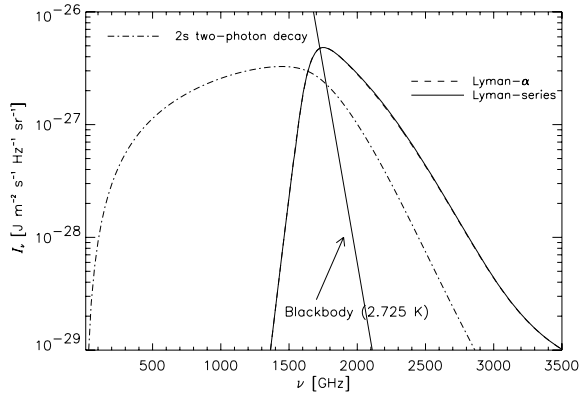

Figure 8. The Lyman series and the 2s two-photon decay spectrum. The main contribution to the Lyman series (thick solid line) comes from the Lyα transition (dashed line). The peak intensities for the first few transitions are $\Delta I_\nu = 4.8 \times 10^{-27}, 2.9 \times 10^{-29}, 4.9 \times 10^{-30}$ and 2.2×10^{-30} J m^{-2} s^{-1} Hz^{-1} sr^{-1} for the Lyα, Lyβ, Lyγ and Lyδ, respectively. For comparison, the 2.725-K blackbody is also shown (thin solid line).

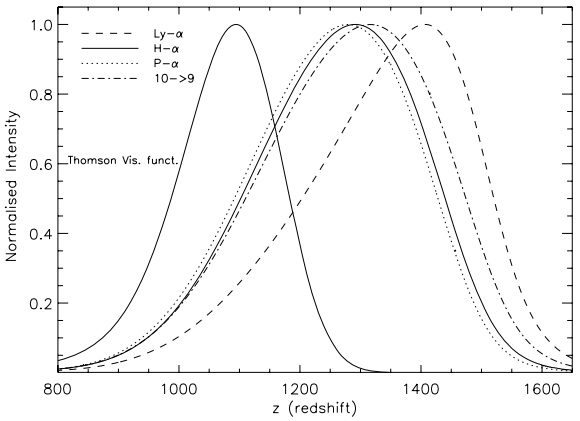

Figure 9. Redshift of formation for different lines. We present the normalized intensity for several transitions with $\Delta n = 1$ as a function of redshift z. For comparison, we also show the Thomson visibility function normalized to unity at the peak, showing that the redshift of formation of the lines is higher than that of formation of the CMB fluctuations.

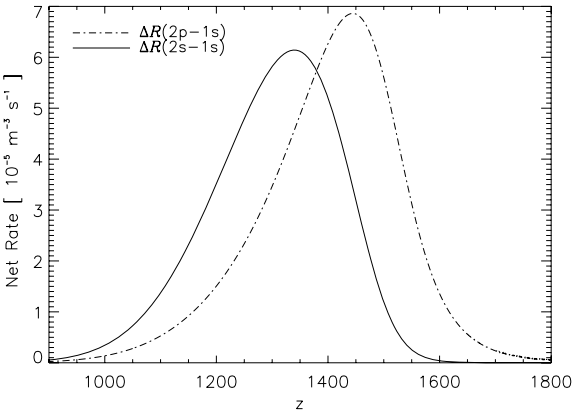

Figure 10. Net rates for transitions from levels $n = 2$ to the ground state. The rate ΔR(2p–1s) mimics the shape of the Lyα line (compare with Fig. 9). Note that the 2s two-photon decay rate dominates for redshifts smaller than ∼1400 (the two rates are equal at $z \sim 1380$), that is, where the bulk of recombination takes place, and where all the contributions from higher transitions originate.

Here, another important point is that observations of these lines permit us to explore an epoch of the Universe, where the optical depth due to Thomson scattering is very high. Note that the effects discussed in Rubiño-Martín et al. (2005) also provide spectral information but, due to the shape of the Thomson visibility function (Sunyaev & Zeldovich 1970a), this information comes from lower redshifts ($z \sim 1100$).

Fig. 10 shows the redshift dependence of the net (radiative) rates of the Lyα and 2s two-photon decay transitions. As it is well-known, the 2s−1s rate dominates during the epoch of recombination, and provides the main channel through which recombination can proceed (Zeldovich et al. 1968). On the other hand, escape through the Lyα line happens at earlier times (the two rates are equal at $z \sim 1380$). Note that due to the narrowness of the Lyα line profile, the shape of ΔR(2p–1s) mimics that of the Lyα contribution to the CMB spectral distortion (compare with Fig. 9).

3.2.1 About the pre-recombination peak

In earlier calculations of the recombination spectrum the existence of a pre-recombination peak for the Lyα transition was found (Rybicki & dell'Antonio 1994; Wong et al. 2006). However, in our calculations we do not find any significant emission from any hydrogen line above redshifts $z \sim 2000$, provided that the primordial radiation field is described by a pure blackbody law.

With the assumption that there are no intrinsic distortions of the CMB spectrum it is expected that at some high redshift the populations of all neutral hydrogen states can be described using the Saha relations, with tiny deviations only coming from the disturbance of equilibrium due to the expansion of the Universe. Clearly, in this case it is impossible to have any uncompensated loops between different levels and hence no significant net emission should occur (Liubarskii & Sunyaev 1983).

Our calculations show that, at redshifts $z \gtrsim 2000$, the net rate of the 2p$-$1s process becomes zero (within the numerical accuracy of the codes, which is much higher than the effects we are discussing here).

We found that here it is very important to obtain the solution for the populations of levels with sufficiently high accuracy. In local thermodynamic equilibrium (LTE), the Saha relation yields

$$\left(\frac{N_j}{N_i}\right)^{\rm LTE} = \frac{g_j}{g_i}\,{\rm e}^{h\nu_{ij}/kT_\gamma} \tag{7}$$

for the ratio of the population of the levels i and j. This ratio evidently is very sensitive to the value of the transition frequency ν_{ij}. Inserting this expression into equation (2) it is clear that analytically one obtains *no* net emission, provided that $\nu_{ij} = \mid \chi_i - \chi_j \mid /h$, with χ_i being the ionization potential of the corresponding level.

However, in *numerical* calculations at sufficiently early epochs one will obtain a solution for the population of each level, which is extremely close to the numerical LTE solution. But in fact, when one now computes $\frac{g_i}{g_j}\left(N_j/N_i\right)^{\rm LTE}_{\rm num}\,{\rm e}^{-h\nu_{ij}/kT_\gamma}$ numerically even deviations of the order of $\Delta(N_j/N_i)^{\rm LTE}_{\rm num}/(N_j/N_i)^{\rm LTE} \sim 10^{-5}$ from the real LTE solution will lead to sizeable *false* emission, when deviations from LTE should be small.

This in principle can occur when using a slightly different value, $\tilde{\nu}_{ij} = \nu_{ij} + \delta\nu_{ij}$ (e.g. from older pre-calculated tables or using different combinations of the natural constants for unit conversions) for the transition frequency in the set-up of the coupled system of ordinary differential equations, while obtaining the output of the recombination spectrum with ν_{ij}. In other words, a false pre-recombination peak appears when one is *not* comparing the obtained numerical solution with the corresponding numerical LTE solution, which in this set-up should fulfil

$$\left(\frac{N_j}{N_i}\right)^{\rm LTE}_{\rm num} = \frac{g_j}{g_i}\,{\rm e}^{h(\nu_{ij}+\delta\nu_{ij})/kT_\gamma}. \tag{8}$$

Inserting this expression into equation (2) one obtains

$$\Delta R^{\rm num}_{ij}(\nu) \propto 1 - {\rm e}^{h\delta\nu_{ij}/kT_\gamma}. \tag{9}$$

Because of the large factor $\kappa = h\nu_{ij}/kT_0$ in the exponent even for $\delta\nu_{ij}/\nu_{ij} \sim 10^{-6}$ this leads to notable *false* emission at early epochs, while leaving the main recombination peak unchanged. As an example, for the Lyα transition ($\kappa \approx 43455$ and $\Delta\nu_\alpha/\nu_\alpha \sim 10^{-6}$) one obtains a pre-recombination emission, which peaks at $z \sim 3100$ with $\Delta I \sim 6 \times 10^{-26}\,{\rm J\,m^{-2}\,s^{-1}\,Hz^{-1}\,sr^{-1}}$, while the recombination peak is roughly 10 times smaller!

One should mention that although at $z > 2000$ there is a small difference in the electron and photon temperature ($\Delta T/T_\gamma \sim 10^{-6}$) this cannot lead to any pre-recombination emission: due to the large entropy of the Universe ($N_{\rm b}/N_\gamma \sim 6 \times 10^{-10}$) one expects that even for a larger $\Delta T/T_\gamma$ the statistics of the hydrogen levels is controlled by the photon field. This implies that in the Boltzmann factors T_γ appears instead of $T_{\rm e}$. It is expected that even the inclusion of collisional processes, which we neglected here, will not change this fact. Similarly, the expected small change in the electron temperature due to Compton heating a distorted photon field will not be of importance. We therefore conclude that there should be no hydrogen pre-recombination emission and that similarly one should not expect any pre-recombination emission from helium.

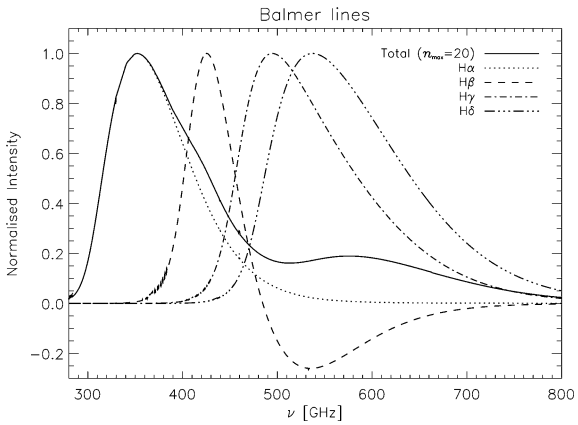

Figure 11. Different contributions to the Balmer series. For convenience, we normalized each of the contributions to unity at their maximum. The normalization factors are $\Delta I_\nu = 6.5 \times 10^{-27}, 7.5 \times 10^{-28}, 4.1 \times 10^{-28}$ and $2.5 \times 10^{-28}\,{\rm J\,m^{-2}\,s^{-1}\,Hz^{-1}\,sr^{-1}}$ for the Hα, Hβ, Hγ and Hδ, respectively.

3.3 The two-photon decay spectrum

In Fig. 8, we also show the contribution due to the 2s two-photon decay. The peak of the emission is roughly at $\nu \sim 1460\,{\rm GHz}$ ($\approx$205 μm) and partially fills the gap between the Lyman and Balmer series (compare with Fig. 1).

The amplitude of the 2s two-photon decay line is approximately $3.3 \times 10^{-27}\,{\rm J\,m^{-2}\,s^{-1}\,Hz^{-1}\,sr^{-1}}$, which is only a factor of $\sim$1.5 times smaller than the peak value of the Lyα line. This ratio is compatible with the result found by Boschan & Biltzinger (1998), while it differs from the result of Wong et al. (2006) by a factor of 2, as a consequence of their different normalization of the profile function.

Fig. 10 also presents the 2s$-$1s net rate as a function of redshift. Note that one cannot directly infer from this figure the position of the peak intensity of the contribution to the CMB spectral distortion due to the 2s decay, because in this case the line profile (which appears in the kernel of integration in equation 3) is very broad. Therefore, the resulting spectral distortion is much broader than any other radiative line ($\Delta\,\nu/\nu \approx 0.8$, which is practically four times larger than the value for Lyα), and it peaks at higher frequencies than in the simple extrapolation of the redshifted central frequency $\nu_{\rm 2s} \sim \nu_{{\rm Ly}\alpha}/2$ (Wong et al. 2006).

3.4 The Balmer transitions and beyond

Fig. 11 shows the different contributions to the Balmer series using a linear scale in intensity. The main contribution comes from the Hα line. One can see that the contribution from Hβ becomes negative in a certain frequency range. The positive

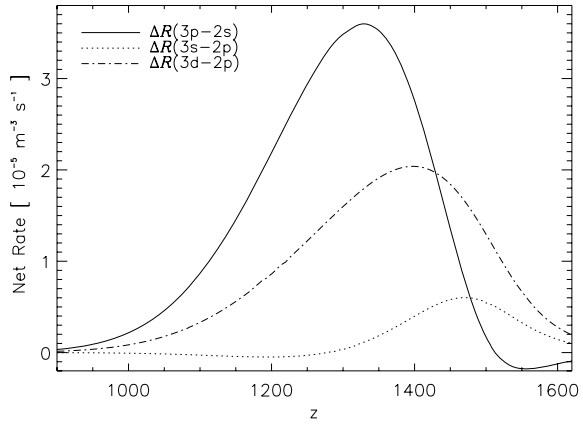

Figure 12. Net rates for transitions from levels $n = 3$ to 2. This figure contains all transitions contributing to the Hα line, namely ΔR(3s–2p), ΔR(3p–2s) and ΔR(3d–2p), except the 3p−1s. However, the contribution of the rate ΔR(3p–1s) to the line is very small (it peaks at $z \sim 1470$ with amplitude 4.6×10^{-7} m^{-3} s^{-1}), so we can omit it. During the epoch of formation of the line, the fastest transition is 3p−2s, and therefore the population of the 3p level will be smaller than the expected equilibrium value (see Fig. 5).

wing of Hβ slightly enhances the high-frequency wing of the main feature at 350 GHz, while the rest of the lines (Hγ and above) add up to produce a secondary peak around 600 GHz, completely compensating the negative part of Hβ. Note that this result differs from that of Dubrovich & Shakhvorostova (2004), where their Hβ and Hγ are both negative, and all the higher transitions do not compensate them. Also in general the amplitude of our results is smaller by a factor of $\sim$10. We also mention that the results of Rybicki & dell'Antonio (1993) for $n_{\rm max} = 10$ contain negative features which are not found in our computations (see Fig. 3).

Fig. 12 shows the net (radiative) rates for all transitions connecting levels $n = 3$ and 2, and which contribute to the Hα line. The fastest rate is associated with the 3p−2s channel, as one would expect because the Hα line forms around $z \approx 1300$ (see Fig. 9), where escape through the 2s−1s channel is faster than through the 2p−1s one.

For higher series, one can perform a similar analysis. For instance, in the left-hand panel of Fig. 13 we show the first contributions ($\Delta n \leqslant 5$) to the series corresponding to level $n = 15$. It is clear that for large values of n, the relative distance between transitions with $\Delta n =$ 1 and 2 increases ($\Delta\nu/\nu \equiv [\nu_{n,n+1} - \nu_{n,n+2}]/\nu_{n,n+1} > 0.8$ for $n \geqslant 13$). Given that the typical width of the lines is of the order of 0.3 (see Table 1), the α-transition is giving a separated peak, while the other transitions of the series overlap and result in a nearly constant emission plateau in the high-frequency wing. Although it is not shown here, we have checked that the slope of this plateau is steeper than the one obtained in the case of $n_{\rm sp} = 2$. The co-added contribution of all these high-frequency wings of all series is contributing to the net slope at low frequencies in Fig. 1.

On the other hand, the peaks coming from the main ($\Delta n = 1$) transition of a given series cannot be separated from those of other series for high values of n, because they start to overlap. In the right-hand panel of Fig. 13, we show this overlapping for the three series corresponding to $n = 14, 15$ and 16. In this case, $\Delta\nu/\nu$ defined as $[\nu_{n,n+1} - \nu_{n+1,n+2}]/\nu_{n,n+1}$ is a decreasing function with n, so $\Delta\nu/\nu \leqslant 0.2$ for $n \geqslant 13$, and thus the peaks start to overlap and merge into a continuum. This effect can be seen in the low-frequency part of Fig. 1. Note that the co-added contributions of all the high-frequency

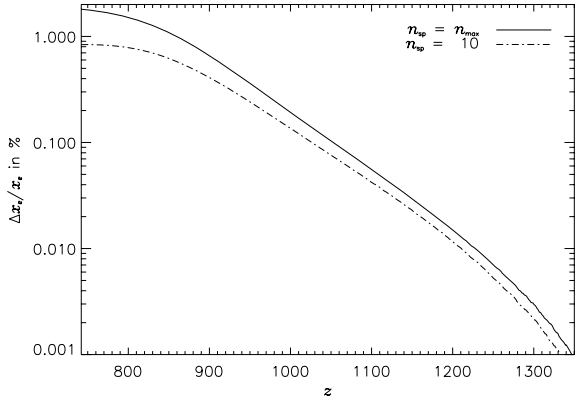

Figure 14. Relative change in the free electron fraction ($x_{\rm e} = N_{\rm e}/N_{\rm H}$). We consider the 25-shell atom and show the relative difference in $x_{\rm e}$ with respect to the standard computation $\{\Delta x_{\rm e}/x_{\rm e} \equiv [x_{\rm e} - x_{\rm e}(n_{\rm sp} = 2)]/x_{\rm e}(n_{\rm sp} = 2)\}$ for two cases: full computation ($n_{\rm sp} = n_{\rm max}$) and $n_{\rm sp} = 10$.

wings are giving the net slope. If the populations of l-substates are not followed, the transitions with $\Delta n > 1$ will be larger, and thus we will have a different behaviour in the asymptotic slope in the subGHz range.

3.5 Non-equilibrium effects of the angular momentum states on the electron fraction

One of the important variables in our calculations is the electron fraction, $x_{\rm e} = N_{\rm e}/N_{\rm H}$, as a function of redshift z. Here, we want to quantify the effects on the electron fraction. To do so, we compare the results obtained for the 25-shell atom in the full calculation ($n_{\rm sp} =$ 25) with those for standard computation ($n_{\rm sp} = 2$). Fig. 14 shows the relative change of the free electron fraction due to the inclusion of angular momentum substates. In the standard computation, the residual electron fraction at low redshifts ($z = 800$) is smaller by $\sim$1.5 per cent than in the case of full l-follow-up, implying that in this case the process of recombination is slightly slower. Note that for $n_{\rm sp} = 10$ one obtains approximately half of the effect.

The net effect during the epoch of recombination ($z_{\rm dec} = 1089 \pm 1$, Bennett et al. 2003) is smaller than 0.1 per cent. Therefore, one would only expect a small impact on the angular power spectrum of the CMB. To quantify this effect we have modified the CMBFAST (Seljak & Zaldarriaga 1996) code, to incorporate the recombination history obtained in our computations. We note that this recombination history is computed inside CMBFAST using the RECFAST (Seager et al. 1999) code, which is based on calculations for a 300-level hydrogen atom in which SE among the l sublevels was assumed (Seager et al. 2000). Our computation makes the assumption that the relative change of the electron fraction, as obtained for the 25-shell atom, will not vary significantly when including more shells. Although the inclusion of more shells in our calculations should still lead to a decrease of the residual electron fraction at low redshifts (one would expect to converge for $n_{\rm max} \sim 50$), we found that the above assumption is justified reasonably well. We will further discuss this point in a future work.

Fig. 15 shows that the relative difference of the C_ℓ is smaller than $\sim$0.5 per cent ($\sim$1.1 per cent) for the TT (EE) angular power spectrum. Following Seager et al. (1999) we can model the results by multiplying the recombination/ionization rates by a 'fudge factor'. Our results for $x_{\rm e}$ are reproduced with an extra factor of 0.967, that is, the fudge factor inside RECFAST should be 1.10 instead of 1.14.

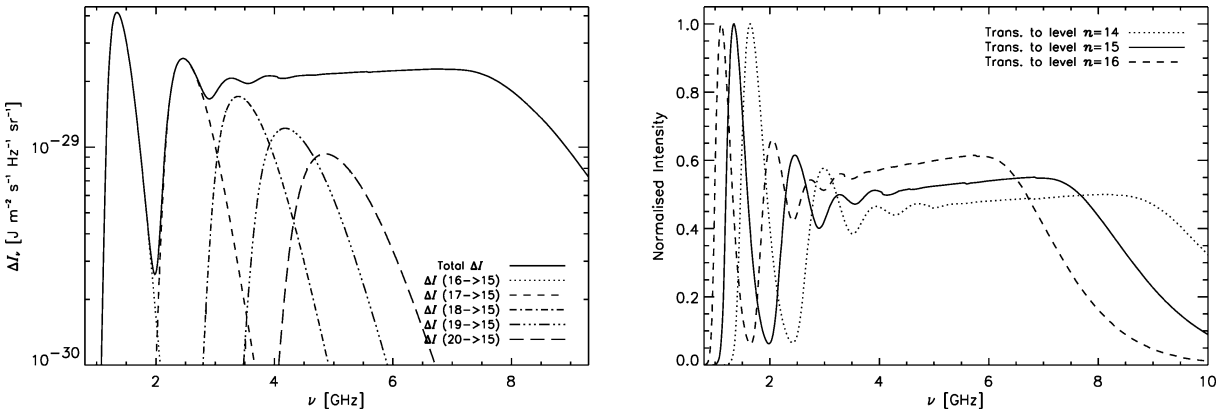

Figure 13. Different contributions to a high-n series. Left-hand panel: we show the contribution of all transitions to level $n = 15$ for a hydrogen atom with $n_{\rm max} = 30$. There is a strong peak produced by the corresponding $\Delta n = 1$ transition, while the rest of transitions ($\Delta n \geqslant 2$) add up to produce a (practically) featureless high-frequency wing of the series. Right-hand panel: we show the net contribution of all transitions to levels $n = 14, 15$ and 16, in normalized intensity units. At frequencies below a few GHz, the contribution of the $\Delta n = 1$ transitions starts to overlap.

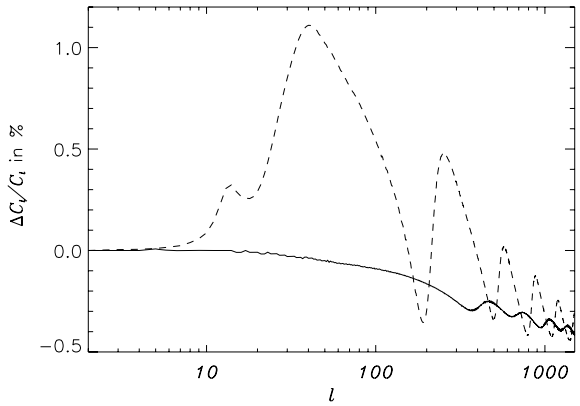

Figure 15. Relative change in the temperature (TT, solid line) and polarization (EE, dashed line) angular power spectra due to the inclusion of detailed follow-up of the angular momentum substates, for the *WMAP* best-fitting cosmological model.

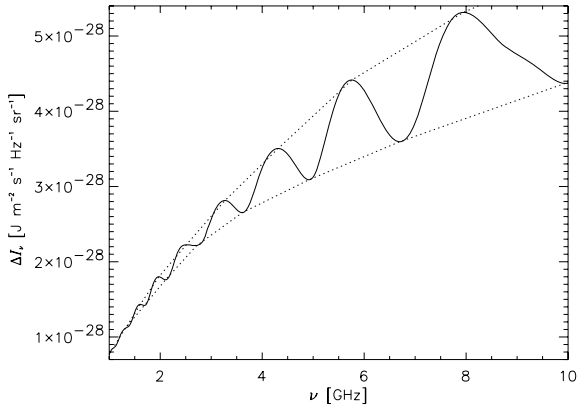

Figure 16. A detail of the hydrogen spectrum in the frequency domain between 1 GHz and 10 GHz. We present in linear scale the amplitude of the features in the region of the spectrum where we expect that detection should be more feasible. Dotted lines are connecting the maxima and minima of the features, so one can read directly their contrast.

Finally, we would like to mention that there are other effects, which may produce small changes in the values of C_ℓ. For example, Chluba & Sunyaev (2006) considered the effect of stimulated emission due to the presence of soft CMB photons on the total 2s-decay rate. In addition, Leung, Chan & Chu (2004) discussed the effect of a modification of the adiabatic index in the matter equation of state as recombination proceeds and Dubrovich & Grachev (2005) included corrections due to the two-photon decay of higher hydrogen levels and helium. All the aforementioned processes lead to changes of the order of 1 per cent and even cancel each other partially, leaving a lot of space for future work and discussion.

4 DISCUSSION

The spectrum of the background radiation of the Universe has a minimum in the vicinity of 30–40 cm (Longair & Sunyaev 1972). It is very impressive that the brightness temperature in the recombinational line component has a maximum relative to the background radiation spectrum precisely in this spectral band (see Fig. 2), and reaches values of the order of 10^{-7}. This is a consequence of the fact that the asymptotic slope of the spectral distortions to the blackbody (which in our case is of the order of $\approx +0.8$) is decaying slower with frequency than the Rayleigh–Jeans part of the CMB (slope $+2$). Note that the turn over at around 0.5 GHz is due to the lack of diffusion from high levels in our calculation with $n_{\rm max} = 30$.

It is extremely difficult to separate an additional continuum component with quasi-flat spectrum from the foreground sources. However, the lines with $\Delta n = 1$ will still influence the shape of the integral curve, and the contribution from recombination is modulated in such a way that no foreground source is able to mimic it. Obviously, one of the most interesting spectral regions corresponds to those frequencies just above 1420 MHz (21-cm line), where the contribution of synchrotron emission of relativistic electrons of radio and ordinary galaxies (e.g. Longair & Sunyaev 1972; Longair 1993) and free–free emission from our Galaxy are not expected to have a quasi-periodic dependence on the wavelength [for a more detailed discussion of foregrounds for 21-cm studies, see Oh & Mack (2003) and Morales, Bowman & Hewitt (2005)].

At low frequencies, the amplitude of this frequency modulation is not strong, but it might become measurable by future experiments (see e.g. Fixsen & Mather 2002). Fig. 16 shows that the contrast

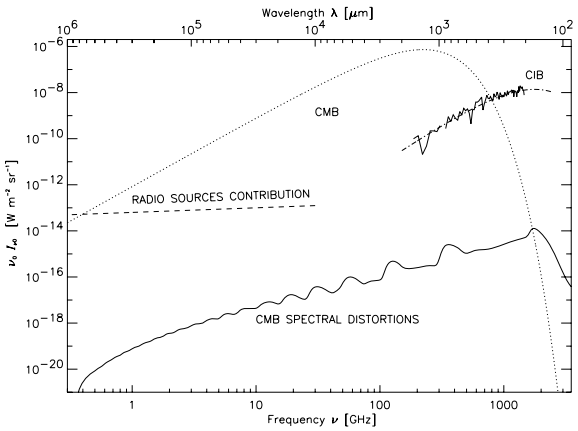

Figure 17. Spectral distortions and foregrounds. We compare the result of Fig. 1 with the pure blackbody spectrum of 2.725 K (dotted line); with the emission of the CIB derived by Fixsen et al. (1998) (dot–dashed line) and Lagache et al. (2000) (solid line between 200 μm and 1.2 mm); and with the estimates of the contribution of extragalactic radio sources from Longair (1993) [note that this refers to the extragalactic sources with an average spectral index of -0.8 in flux, and which roughly scales as 6 K $\times$ $(\nu/178\,\mathrm{MHz})^{-2.8}$; this is why in these coordinates, their contribution seems practically flat].

of these features in the frequency range between 1 and 10 GHz is between 5 and 30 per cent. Even though the amplitude of these features may still increase when considering larger values of $n_{\rm max}$, the contrast should not change significantly. Note that the Balmer, Paschen and Brackett series have a higher contrast and they are found in the frequency band where the contamination is smaller, but they will be much more difficult to observe because they lie two orders of magnitude below in relative intensity (see Fig. 2). We would like to mention here that there have been observational efforts to measure the CMB spectrum at centimetre wavelengths (Fixsen et al. 2004; Kogut et al. 2004), searching for signatures of spectral distortions from early energy injection in the spectrum (Sunyaev & Zeldovich 1970b; Illarionov & Syunyaev 1975).

Although the Lyα distortion is the strongest feature in the spectrum (relative distortion in the peak is of order unity), the CIB in this region is dominant, making its observation extremely difficult. However, the sensitivity of the detectors is improving a lot, so these observations could become feasible in the future. For example, the recent measurements of Spitzer (Dole et al. 2006) have shown that at 160 μm, practically three quarters of the mid-infrared background (MIB) can be already resolved into luminous infrared galaxies at $z \sim 1$. If the MIB could be completely resolved, one might be able to remove the source contamination in a given piece of sky in order to measure the spectral distortions discussed here.

For illustration, Fig. 17 shows the amplitude of the spectral distortions compared to the determination of the CIB obtained with *COBE* FIRAS data (Fixsen et al. 1998), and the result of Lagache et al. (2000) in the Lockman Hole using the WHAM Hα survey and the Leiden/Dwingeloo H I data. We note that, in addition to the CIB signal, there will be also a strong contamination from our Galaxy (see the discussion in Wong et al. 2006).

We would like to stress that all the results of this work were obtained within the standard framework which has been adopted by many other authors working on this topic (see the references in Section 1). The main difference with respect to these earlier works is the detailed treatment of the l-substates. However, it is clear that one has to evaluate the impact of other physics which has been neglected so far. As an illustration, we will discuss three additional physical processes which have not been included here and which could modify the results.

The first effect is connected with collisions. Although the collisional rates are smaller than the radiative rates during the epoch of recombination (Seager et al. 2000), they could produce a redistribution of electrons if we consider states which are not directly connected via dipolar electric transitions (e.g. collisions can produce transitions of the type $(n,\, l) \rightarrow (n,\, l')$ also for $\Delta l \neq 1$). In principle, this effect should be important for shells with large principal quantum number n, and would tend to restore SE, thus restoring the $(2l + 1)$ ratios of the populations of the levels within a given shell. In other words, one should eventually recover the non-splitting solution for sufficiently high shells, and the asymptotic slope of $+0.35$ found by Kholupenko et al. (2005) might be reached. One can do a simple estimate of the effect by using the collisional rates described by equation (43) of Pengelly & Seaton (1964). In our problem, the collisional transition probability $q_{nl} N_{nl} N_{\rm e}$ becomes of the order of the radiative transition probability A_{nl} for $n \gtrsim 25$–30 at the redshift of formation of the lines ($z \approx 1300$). Thus, if one wants to include a higher number of shells in the computations, the effect of collisions on the mixing of the populations in different l-sublevels has to be taken into account.

The second effect is the free–free absorption (see e.g. Illarionov & Syunyaev 1975; Dubrovich & Shakhvorostova 2004), which at low frequencies will tend to restore the blackbody with $T_\gamma = T_{\rm e}$ and thus will erase the features in the spectrum. However, this effect will be only important for high shells, so our computation up to $n_{\rm max} = 30$ will not change significantly.

Finally, also the inclusion of additional radiative channels (stimulated two-photon decay from higher levels, forbidden transitions, i.e. both electric and magnetic quadrupole transitions, or magnetic dipole transitions) may have some impact on the computed spectral distortions. However, we would expect that the inclusion of these new channels will not substantially modify the spectral distortions discussed here. The reason for this is that all the sublevels with $n > 2$ can connect to lower states via permitted radiative transitions having escape probability very close to unity. Therefore, the inclusion of additional 'slow channels' should only modify our results at the level of a few per cent. We have already checked that the inclusion of stimulated 2s two-photon decay (Chluba & Sunyaev 2006) and some additional two-photon decay channels for higher hydrogenic levels (following the prescription in Dubrovich & Grachev 2005), leads to differences with respect to our computations of the order of 1 per cent, in both the recombination spectrum and the electron fraction.

Certainly one should try to develope an approach including all the aforementioned processes stimultaneously, but this will be left for a future work.

5 CONCLUSIONS

In this paper, we have computed the spectral distortions of the CMB frequency spectrum originating from the epoch of cosmological hydrogen recombination, by following the evolution of the populations of the levels of a hydrogen atom with $n_{\rm max} = 30$ in the redshift range from $z = 3500$ down to $z = 500$. Our computation follows in detail the evolution of all angular momentum substates. This permits us to describe the non-equilibrium effects which appear during the process of recombination in the populations of the sublevels.

The populations of the levels are found to differ (with respect

to the standard computation without detailed follow-up of l-states) by more than 20 per cent for low redshifts ($z \lesssim 800$). In addition, the amplitude of the lines is also affected. Following all the angular momentum substates, the relative ratio of the different lines within a given series increases. This can be seen, for example, in the case of the Balmer series, where the amplitude of the α-transition ($\Delta n = 1$) increases while the rest of transitions decrease. This shows that the simplifying assumption of SE within a given shell leads to an overall underestimation of the net emission at high frequencies.

We have also quantified the effects on the residual electron fraction, showing that at low redshifts ($z \approx 800$) the $x_{\rm e}$ is increased by 1.5 per cent. The impact of this change on the angular power spectrum is small, producing differences of the order of 1 per cent in the values of C_ℓ.

Finally, our computations have shown that, if the primordial radiation field is assumed to be a pure blackbody spectrum, then there is no significant emission from any line for redshifts greater than $z = 2000$, so a 'pre-recombination' peak does not exists.

ACKNOWLEDGMENTS

We acknowledge use of the CMBFAST software package (Seljak & Zaldarriaga 1996). JAR-M acknowledges the hospitality of the MPA during several visits, and thanks Andrés Asensio Ramos for useful discussions. JC thanks the IAC for hospitality during his visit in 2006 March. We also thank our referee, Douglas Scott, for his useful remarks and his interest in this paper.

REFERENCES

Bennett C. L. et al., 2003, ApJS, 148, 1
Boardman W. J., 1964, ApJS, 9, 185
Boschan P., Biltzinger P., 1998, A&A, 336, 1
Burgess A., 1958, MNRAS, 118, 477
Burgin M. S., 2003, Astron. Rep., 47, 709
Chluba J., Sunyaev R. A., 2006, A&A, 446, 39
Chluba J., Rubino-Martin J. A., Sunyaev R. A., 2006, MNRAS, submitted (astro-ph/0608242)
Dole H. et al., 2006, A&A, 451, 417
Dubrovich V. K., 1975, Pis ma Astronomicheskii Zhurnal, 1, 3; English transl., 1975, Sov. Astron. Lett., 1, 196
Dubrovich V. K., Stolyarov V. A., 1995, A&A, 302, 635
Dubrovich V. K., Stolyarov V. A., 1997, Astron. Lett., 23, 565
Dubrovich V. K., Grachev S. I., 2004, Astron. Lett., 30, 657
Dubrovich V. K., Shakhvorostova N. N., 2004, Astron. Lett., 30, 509
Dubrovich V. K., Grachev S. I., 2005, Astron. Lett., 31, 359
Fixsen D. J., Mather J. C., 2002, ApJ, 581, 817
Fixsen D. J., Cheng E. S., Gales J. M., Mather J. C., Shafer R. A., Wright E. L., 1996, ApJ, 473, 576
Fixsen D. J., Dwek E., Mather J. C., Bennett C. L., Shafer R. A., 1998, ApJ, 508, 123
Fixsen D. J., Kogut A., Levin S., Limon M., Lubin P., Mirel P., Seiffert M., Wollack E., 2004, ApJ, 612, 86
Illarionov A. F., Syunyaev R. A., 1975, Sov. Astron., 18, 691
Karzas W. J., Latter R., 1961, ApJS, 6, 167
Kholupenko E. E., Ivanchik A. V., Varshalovich D. A., 2005, Gravitation and Cosmology, 11, 161
Kogut A., Fixsen D. J., Levin S., Limon M., Lubin P. M., Mirel P., Seiffert M., Wollack E., 2004, ApJS, 154, 493
Lagache G., Haffner L. M., Reynolds R. J., Tufte S. L., 2000, A&A, 354, 247
Leung P. K., Chan C. W., Chu M.-C., 2004, MNRAS, 349, 632
Liubarskii I. E., Sunyaev R. A., 1983, A&A, 123, 171
Longair M. S., Sunyaev R. A., 1972, Sov. Phys. Uspekhi, 14, 569
Longair M. S., 1993, in Calzetti D., Livio M., Madau P., eds, Proc. STScI Symp., Extragalactic Background Radiation: A Meeting in Honor of Riccardo Giacconi. Cambridge Univ. Press, Cambridge, p. 223
Mather J. C. et al., 1994, ApJ, 420, 439
Morales M. F., Bowman J. D., Hewitt J. N., 2005, BAAS, 37, 1217
Nussbaumer H., Schmutz W., 1984, A&A, 138, 495
Oh S. P., Mack K. J., 2003, MNRAS, 346, 871
Peebles P. J. E., 1968, ApJ, 153, 1
Pengelly R. M., Seaton M. J., 1964, MNRAS, 127, 165
Rubiño-Martín J. A., Hernández-Monteagudo C., Sunyaev R. A., 2005, A&A, 438, 461
Rybicki G. B., dell'Antonio I. P., 1993, in Chincarini G., Iovino A., Maccacaro T., Maccagni D., eds, ASP Conf. Ser. Vol. 51, Observational Cosmology. Astron. Soc. Pac., San Francisco, p. 548
Rybicki G. B., dell'Antonio I. P., 1994, ApJ, 427, 603
Seager S., Sasselov D. D., Scott D., 1999, ApJ, 523, L1
Seager S., Sasselov D. D., Scott D., 2000, ApJS, 128, 407
Seljak U., Zaldarriaga M., 1996, ApJ, 469, 437
Sobolev V. V., 1946, Moving Atmospheres of Stars. Leningrad State Univ., Leningrad; English transl., 1960, Harvard Univ. Press, Cambridge
Spergel D. N. et al., 2003, ApJS, 148, 175
Spergel D. N. et al., 2006, ApJ, preprint (astro-ph/0603449)
Spitzer L. J., Greenstein J. L., 1951, ApJ, 114, 407
Storey P. J., Hummer D. G., 1991, Comput. Phys. Commun., 66, 129
Sunyaev R. A., Zeldovich Y. B., 1970a, Ap&SS, 7, 3
Sunyaev R. A., Zeldovich Y. B., 1970b, Ap&SS, 7, 20
Wong W. Y., Seager S., Scott D., 2006, MNRAS, 367, 1666
Zeldovich Y. B., Kurt V. G., Syunyaev R. A., 1968, ZhETF, 55, 278

This paper has been typeset from a TEX/LATEX file prepared by the author.